

Modeling Hypertrophic IP3 Transients in the Cardiac Myocyte

Michael Cooling,* Peter Hunter,* and Edmund J. Crampin*[†]

*Auckland Bioengineering Institute and the [†]Department of Engineering Science, University of Auckland, New Zealand

ABSTRACT Cardiac hypertrophy is a known risk factor for heart disease, and at the cellular level is caused by a complex interaction of signal transduction pathways. The IP₃-calcineurin pathway plays an important role in stimulating the transcription factor NFAT which binds to DNA cooperatively with other hypertrophic transcription factors. Using available kinetic data, we construct a mathematical model of the IP₃ signal production system after stimulation by a hypertrophic α -adrenergic agonist (endothelin-1) in the mouse atrial cardiac myocyte. We use a global sensitivity analysis to identify key controlling parameters with respect to the resultant IP₃ transient, including the phosphorylation of cell-membrane receptors, the ligand strength and binding kinetics to pre-coupled (with G_αGDP) receptor, and the kinetics associated with precoupling the receptors. We show that the kinetics associated with the receptor system contribute to the behavior of the system to a great extent, with precoupled receptors driving the response to extracellular ligand. Finally, by reparameterizing for a second hypertrophic α -adrenergic agonist, angiotensin-II, we show that differences in key receptor kinetic and membrane density parameters are sufficient to explain different observed IP₃ transients in essentially the same pathway.

INTRODUCTION

Pathological cardiac hypertrophy has been identified as a major risk factor leading to heart failure (1). An understanding of the biological pathways involved in cardiac hypertrophy may yield benefits in understanding the progression of, and the development of therapies for, cardiac disease.

A range of signal transduction pathways are implicated in hypertrophy, including the inositol 1,4,5-trisphosphate (IP₃)-calcineurin pathway, the mitogen-activated protein kinase p42/p44, mitogen-activated protein kinase p38, jun N-terminal kinase, and the phosphoinositide 3-kinase-wingless-related mouse mammary tumor virus integration (PI3K-Wnt) pathways (2–10). In vivo, none has a monopoly on hypertrophic effects and many pathways interact (3), the details of which have yet to be fully elucidated experimentally.

The role of the IP₃-calcineurin pathway in cardiac hypertrophy was discovered during the 1990s and, despite some initial controversy, calcineurin's role has now been accepted. Extracellular agonists stimulate G_q-family G-protein-coupled receptors (GPCRs). On stimulation, the G-protein α -subunit activates phospholipase C (PLC) (11,12), and causes hydrolysis of membrane-bound phosphatidyl inositol-4,5-bisphosphate (PIP₂). This forms the secondary messenger IP₃. IP₃ production causes an increase in the intracellular calcium concentration ($[Ca^{2+}]_i$), which in turn activates the phosphatase calcineurin. Calcineurin activation leads to changes in gene expression by facilitating translocation to the nucleus of cytosolic transcription factors of the nuclear factor of activated T cells (NFAT) family. These such factors bind to nuclear DNA cooperatively with transcription factors from the other hypertrophic pathways to facilitate transcription (13). NFAT's

ability to act as a signal integrator for hypertrophy (14) in this manner is a key reason that the IP₃-calcineurin pathway is significant.

These findings have motivated the use of existing immunosuppressive calcineurin inhibitors (such as Cyclosporin A and FK506) as experimental attenuators of hypertrophy. The results of that approach have been conflicting, with similar rodent models exhibiting no effect, attenuation, or even complete prevention of hypertrophy, and occasionally lethal side-effects from the immunosuppressors (15). Thus, a more detailed understanding of the pathways for hypertrophy is necessary for the development of practical therapeutic treatments.

The biological processes of the IP₃ production system represent only a tiny proportion of the activities within a cell, yet even these are complex with many players and diverse interactions. For such systems a computational model is a useful tool (16), bringing together quantitative and qualitative data to allow interactive exploration of our understanding. Currently no mathematical model for the IP₃-calcineurin pathway exists in the cardiac myocyte.

This work focuses on modeling the signal transduction pathway from extracellular agonist to the production of IP₃ by the extracellular agonists endothelin-1 (17) (ET-1) and angiotensin-II (18) (Ang-2). The responses of IP₃ to the two agonists are different, despite the signal transduction pathway being almost identical. We construct the first mathematical model of the IP₃ production and degradation signal transduction system in the mouse atrial cardiac myocyte, as stimulated by the hypertrophic agonist ET-1. Sensitivity analysis was undertaken to determine which parameters are significant in determining features of the IP₃ transient. We investigate possible causes of the different IP₃ response from stimulation with Ang-2, and show that the differences in system behavior are explainable in terms of receptor kinetics.

Submitted April 2, 2007, and accepted for publication July 18, 2007.

Address reprint requests to M. Cooling, Tel.: 64-9-373-7599, ext. 82165; E-mail: m.cooling@auckland.ac.nz.

Editor: Raimond L. Winslow.

© 2007 by the Biophysical Society
0006-3495/07/11/3421/13 \$2.00

doi: 10.1529/biophysj.107.110031

METHODS

We constructed a mathematical model of the IP₃ production system as stimulated by the α -adrenergic agonist ET-1 in the atrial cardiac myocyte. Since experimental processes are often time consuming and costly, it is important to assess from current knowledge what the most influential parameters are that determine properties of the system. We applied a global sensitivity analysis (the Morris Method) to determine the important parameters of the system by their influence on five characteristics of stimulated IP₃ transients.

Using the ET-1 model as a baseline, we then refined the model to stimulation with the alternative agonist Ang-2. Ang-2 is a hormone produced via the angiotensin-renin system, and also produced locally on stretch of the cardiomyocyte (18,19). Ang-2 signals are received by two main isoforms of the Ang-2 receptor-Type 1 (AT-1) and Type 2 (AT-2). Cells from different animals contain different proportions of each although the proportion is approximately equal in rodents such as the rat (20). There is evidence linking AT-1 receptors to PLC β , IP₃ production, and calcium release via G_q family GPCRs (21–23). Transients resulting from stimulation with Ang-2 are much shorter-lived than those from ET-1, despite the fact that the same pathway is activated in both cases. We sought to determine whether the different transient behavior between the two agonists can be explained in our model by altering key parameters of the receptor alone. We found that the necessary changes to the model could be both motivated and understood by considering the results of the previously completed sensitivity analysis.

Model construction

We developed a mathematical model of the significant biological processes relating to the transduction of extracellular ligand signals through G_q family receptors and subsequent IP₃ production in the mouse atrial cardiac myocyte. A reaction scheme of the model is shown in Fig. 1. The model encompasses the extracellular ligand (*L*), the GPCRs (*R*), activation of phospholipase C β (*P*) by G_qGTP (*G*) subunits, and both the basal and stimulated hydrolysis of PIP₂ to form IP₃. Conceptually, the model can be divided into three modules:

1. GPCR cycling, dealing with ligand, receptors, and diffusible G_q messengers.
2. PLC β cycling, dealing with the activation of PLC β .
3. IP₃ production and degradation, concerned with the hydrolysis of IP₃ from PIP₂, and the background consumption of IP₃.

The mathematical model was formulated using mass action kinetics, and implemented as a system of ordinary differential equations. For convenience, the model was encoded into the computer-readable protocol Cellular modeling Markup Language (CellML) (24). A complete list of the model equations, and a list of model parameters and initial conditions are provided in Tables 3 and 4, respectively. This signal transduction pathway involves interactions between membrane-bound and freely diffusing cytosolic species. Cytosolic species are represented by concentration (in μ M) while

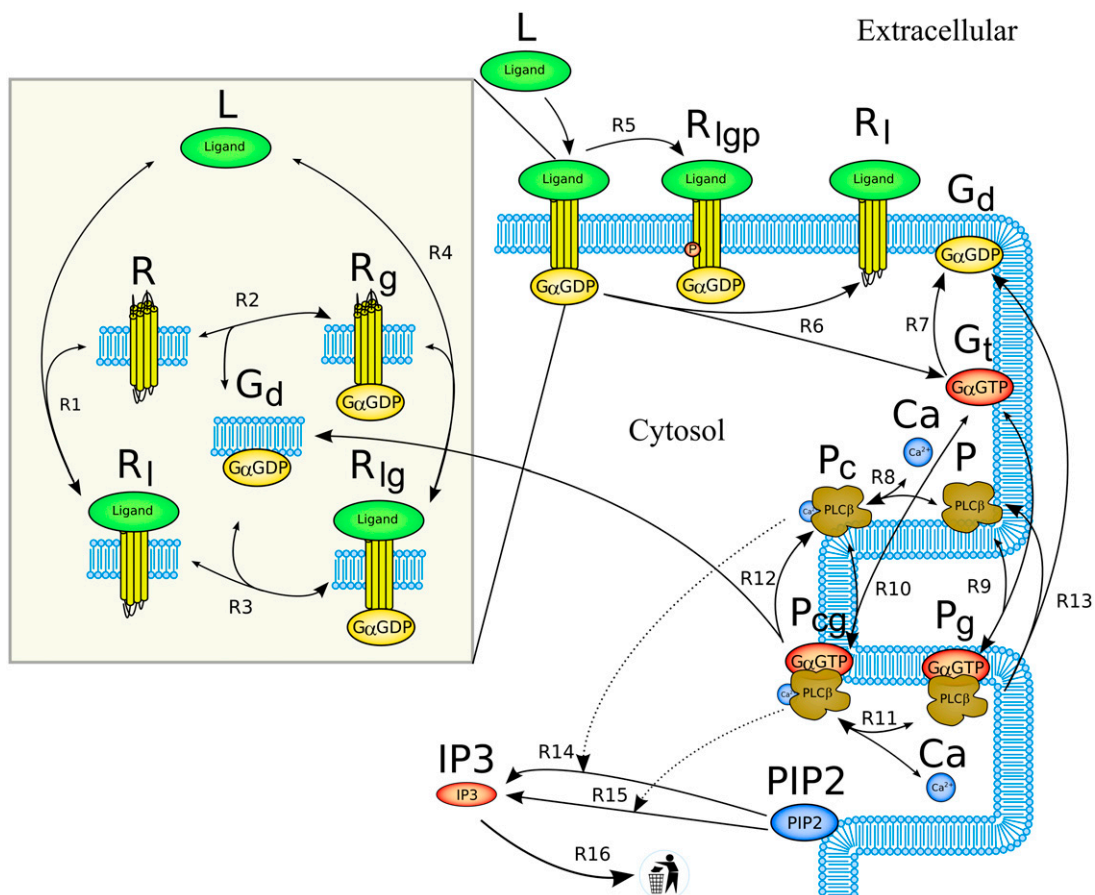


FIGURE 1 Reaction scheme of the IP₃ production system. The extracellular ligand (*L*) binds to receptors (*R*), whether precoupled with G_αGDP (*G_d*, yielding *R_{1g}*) or not (*R₁*). Fully activated receptors (*R_{1g}*) release G_αGTP (*G_t*), which, along with calcium (*Ca*), stimulates PLC β (*P*). In the unstimulated state, PLC β -Ca²⁺ (*P_c*) hydrolyzes PIP₂ to produce IP₃ via reaction R14. When stimulated, PLC β -Ca²⁺-G_αGTP (*P_{cg}*) hydrolyzes PIP₂ at a faster rate via reaction R15. Free IP₃ is degraded via reaction R16.

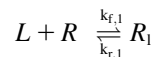
membrane-bound species are given as area densities (number per unit of membrane area, in μm^{-2}). The model is also available as CellML code in the online CellML Repository (<http://www.cellml.org/models>).

GPCR cycling

Extracellular ligand (L) binds to cell-surface receptors (R), shown by reversible reactions $R1$ and $R4$ in Fig. 1. For G_q family receptors, this binding causes a conformational change which replaces GDP with a GTP on an attached G-protein's α -subunit. This causes the G_α subunit to dissociate (reaction $R6$) and stimulate other proteins inside the cell. For a receptor to transduce the ligand signal across the membrane, it requires both an attached G-protein and a ligand-binding event. The model utilizes the receptor components from a nonexcitable cell model of Lukas (25) that uses the precoupled-receptor concept (26): should the G_α subunit bind first (as shown in reaction $R2$), then the receptor is known as precoupled (R_2), and exhibits a higher affinity for the ligand than if G_α had bound after the ligand (via reaction $R3$). Only the state where both ligand and G_α subunit are bound is considered an activated receptor (R_{1g}). Active receptors are targeted for phosphorylation and eventual invagination and recycling by the cellular machinery. Once phosphorylated, the receptor is no longer available for further signal transduction. For the purposes of the model, this is abstracted into a one-time phosphorylation step (reaction $R5$).

The model is designed to simulate experiments where the cell is initially unstimulated. At a predetermined stimulation timepoint (t_s), ligand is added, which is represented by a (smoothed) Heaviside step function to the desired stimulation concentration (L_s). The amount of ligand bound to receptors is assumed negligible compared to the total amount of ligand available, hence the concentration of free ligand in the model does not decrease as ligand binds to the receptors.

All reactions were modeled as kinetic fluxes following the Law of Mass Action. For example, the flux (J_1) for reaction $R1$



is given by the flux expression

$$J_1 = k_{f,1} \times R \times L - k_{r,1} \times R_1,$$

where R is the receptor area density in μm^{-2} , L is the extracellular ligand concentration in μM , R_1 is the density of receptors with ligand bound in μm^{-2} , and $k_{f,1}$ and $k_{r,1}$ are rate constants measured in $\mu\text{M}^{-1} \text{s}^{-1}$ and s^{-1} , respectively. J_1 is therefore a flux measured in $\mu\text{m}^2 \text{s}^{-1}$.

Endothelins bind to their receptors with high enough affinity for the reaction to be considered irreversible under physiological conditions (27), hence it seems likely that when the active G_α subunit dissociates during reaction $R6$, the ligand and receptor complex (R_1) remains together.

PLC β cycling

The active G_α GTP messenger (G_t) released from stimulated receptors binds to the enzyme PLC β (P), shown in Fig. 1 as the reversible reactions $R9$ and $R10$. This binding can be considered independently from the binding of the costimulatory calcium ions (Ca) shown in reversible reactions $R8$ and $R11$. Free G_α GTP degrades to G_α GDP via a self-GTPase activity of the α -subunit, removing its ability to stimulate PLC β , represented as reaction $R7$. This activity in PLC β -bound G_α GTP and dissociation from PLC β is assumed for modeling purposes to occur in the same step and is shown by reactions $R12$ and $R13$ depending on whether Ca^{2+} is also bound or not. When bound to PLC β , this step is assumed to occur at the same rate, irrespective of the additional presence or absence of bound calcium (from P_{cg} or P_g , respectively).

The formulation of the reactions $R7$ - $R13$ follows the same form described in GPCR cycling above, although for some reactions an additional conversion factor is required: Ca^{2+} is a cytosolic species, measured in μM whereas

the membrane-associated fluxes such as J_1 above are membrane density fluxes ($\mu\text{m}^{-2} \text{s}^{-1}$). To convert to concentration fluxes, it is convenient to define a conversion factor

$$C_{pc} = \frac{C_c}{C_p}, \quad (1)$$

where C_c is a conversion factor from a number of particles to a cytosolic concentration (μM), and C_p is a conversion factor from a number of particles to a density on the cell's plasma membrane (μm^{-2}). Together they give a conversion factor that can be applied to the appropriate density fluxes to give the corresponding concentration fluxes for cytosolic products, or vice versa.

A number of parameters were taken from the existing model by Lukas (25), where appropriate. For the binding of Ca^{2+} to PLC β - G_α GTP (Ca binding to P_g in reaction $R11$) only the dissociation constant ($K_{d,11}$) was known. We have made the assumption that the forward rate constant for reaction $R11$ is twice that of the similar reaction $R8$, due to the binding of G_α GTP. From this assumption the reverse rate constant for reaction $R11$ was calculated.

The resting level of calcium in the cardiac myocyte was assumed to be 100 nM (28).

IP3 production and degradation

The species PLC β - Ca^{2+} (P_c) and PLC β - Ca^{2+} - G_α GTP (P_{cg}) act as hydrolyzers, converting the substrate PIP2 to IP3, shown by reactions $R14$ and $R15$ in Fig. 1, respectively. These catalytic reactions were modeled using Michaelis-Menten kinetics according to the quasi-steady-state approximation, their equations therefore being of the form (J_{14} is shown as an example)

$$J_{14} = k_{f,14} \times P_c \times \frac{PIP2}{\left(\frac{K_{m,14}}{C_{pc}} + PIP2\right)},$$

where the K_m of the reaction is scaled by the conversion factor C_{pc} (see Eq. 1).

IP3 binds to IP3 receptors (IP3Rs) in the cell, which are also regulated by calcium. It was assumed that the amounts of both IP3 and calcium bound are negligible compared to their cytosolic concentrations, and therefore IP3Rs do not effect the concentrations of those small species. IP3R activation causes a minor cytosolic calcium spike from intracellular stores, followed by a much larger sustained calcium influx from outside the cell—this latter phenomenon being known as capacitative calcium entry (29). In the protocol of interest to this work, the extracellular entry does not occur, and the minor initial spike is assumed to have little effect on the model calcium. The IP3Rs, having no effect on the rest of the model, are therefore not included in this formulation.

The hydrolysis of PIP2 also produces the membrane-bound diacylglycerol species, but that is not considered in this model.

PIP2 is manufactured by the cell, and resupplied after use to the plasma membrane via the breakdown of inositol phosphates (30). Since there is no evidence that the level of PIP2 is rate-limiting (31), in the model PIP2 is fixed at its initial value.

A degradation reaction ($R16$) encompasses the dephosphorylation or phosphorylation of IP3 to form inositol bisphosphate and inositol tetraphosphate, respectively. For the purposes of this model, the metabolic recycling of IP3 from those products is not considered. The basal level of IP3 is therefore a balance between the basal production and the degradation rates (reactions $R14$ and $R16$, respectively).

A published report (32) of a ~ 30 nM peak in IP3 on stimulation by 100 nM of ET-1, together with estimates of the peak-to-basal ratio of $\sim 2:1$ (33,34), suggest that the basal concentration of IP3 in the mammalian myocyte is ~ 15 nM. This is the estimate used in this model. The kinetics of the basal IP3 production reaction (via $k_{f,14}$) were adjusted to provide this value. The balancing degradation rate was known with more confidence and kept as in the literature (25).

Morris analysis

The model was refined to simulate the response to ET-1 stimulation (see Results for a comparison of model behavior to experimental data). We then sought to determine which parameters controlled the IP3 transient produced by the system by undertaking a global sensitivity analysis following the Morris method (35). The Morris method is a screening algorithm: it ranks the parameters of the model, by their average effect on a particular model simulation output, over a given range of parameter values. The global nature of the analysis is applicable given the system's high nonlinearity (36) and the method has been shown to be as efficient as commonly-used variance based techniques in detecting factors of low sensitivity. It is also computationally cheaper than such techniques (37) as the required number of model evaluations varies linearly with the number of model factors.

The method yields a score for each parameter of the model estimating the partial differential of an objective function with respect to that parameter. We chose five objective functions to analyze the model by, to capture the behavior of the resulting IP3 transient (these measures are illustrated graphically on a representative IP3 transient in Fig. 4):

Baseline Concentration. The basal concentration of IP3 established at steady state before stimulation.

Time-to-Peak. Time in seconds from the stimulation time to the peak IP3 concentration.

Peak Concentration. The maximum concentration of IP3 during the transient.

Tau-to-Tail Ratio. The ratio of the time after the peak at which the tail of the transient dips below $1/e$ of its peak amplitude, to the length of the tail (from the peak to the return to baseline as in the next objective function). Flatter transients have a higher Tau-to-Tail Ratio, closer to 1.0.

Time-to-Baseline. The time in seconds, since stimulation, for the return to baseline concentration. Since returning transients can approach the baseline asymptotically, we measured returning to baseline as occurring when the amplitude of the transient had dropped below 10% after the peak.

To determine the sensitivity of these measures to the model parameters, we define for each parameter a range of values over which it can vary. These may vary widely, whether by virtue of the very different quantities which they represent, or simply by different physiological constraints. The amount of variation of a parameter inside a particular range is normalized to a fraction of that range, designated δ . The parameter ranges defined for our analysis are listed in Table S1 in the Supplementary Material. Parameter ranges were normalized and parameters allowed to take one of 16 equally spaced values (Morris parameter $p = 16$). For each parameter, changes in each of the objective functions were measured for a δ change over the range defined, where δ is (38)

$$\delta = \frac{p}{2} \times \frac{1}{(p-1)}.$$

This yields a sliding window of 53.3% of each parameter's range. Parameters therefore begin each of a series of analysis trajectories at one of 16 values within their defined range, and at each step of each trajectory, one parameter is varied by 53.3% of that range, and the subsequent effect on each the objective functions are measured.

Parameter change effects are divided by δ , to give an estimate for the parameter's effect on each objective measure, over the parameter's entire defined range. We ran two sets of 8000 trajectories as described by Morris (35) for each parameter over the five objective functions (Morris parameter $r = 8000$), as we found this gave repeatable clustering and ordering (unless parameters were very similar in significance) results between the two sets.

For each test, the model was run to achieve steady state before agonist stimulus was applied. Up to a further 130,000 s was simulated (~ 36 h) to allow IP3 to peak and resume the baseline level again for all parameter sets tested.

We then combined both sets of tests to give an overall population for each parameter of 16,000 sensitivity measures, and used the Campolongo ex-

pression (38) of the method to calculate the mean absolute effect (μ^*) as a direction-independent measure of sensitivity of the defined normalized ranges.

Tables S2–S6 in the Supplementary Material show the parameters ranked by their effects thus calculated, for each of the five objective functions.

Angiotensin-II refinement

We sought to determine whether the different IP3 transient produced by Ang-2 (as opposed to ET-1) stimulation could be explained by receptor-related parameters alone. A number of model parameters were therefore adjusted to match known published kinetics for the Ang-2 receptors. It is known that the rodent Ang-2 receptor has a larger dissociation constant than the ET-1 receptor: ~ 1.5 nM in rat and ferret, and that the receptor density is much lower than that for ET-1, being approximately one-fifth (see Table 25 in (28)). These literature-motivated parameter changes alone were not sufficient to explain the differences in the resulting IP3 transient. We therefore investigated the most significant remaining receptor-related parameters.

We used the results of the sensitivity analysis to identify the 10 most significant parameters with respect to the IP3 transient (see Table 1). Two of these ($k_{f,4}$ and $k_{f,5}$) relate to kinetics associated with the receptors themselves, and hence are likely to be different between ET-1 and Ang-2 receptors.

Experimental research by Abdellatif et al. (39) measured accumulation of IP3 in cultured rat neonatal ventricular cardiac myocytes on stimulation of 100 μ M Ang-2, using ion-exchange chromatography. During fitting to this data, we determined predicted new values for those significant receptor parameters using the Levenburg-Marquardt algorithm (implemented as the "levmar" nonlinear least-squares fitting package obtained from <http://www.ics.forth.gr/~lourakis/levmar>). Multiple runs were conducted in an attempt to evade local minima, and a close fit with the experimental data was obtained. Varying additional parameters did not significantly increase the goodness-of-fit.

RESULTS

IP3 transients in response to ET-1 stimulation

Model parameters were refined to the mouse atrial myocyte by fitting the IP3 transient resulting from stimulation at various ET-1 strengths to experimental data from Jiang et al. (40). Based on the available data, we performed the fit based on IP3 transient observations. To our knowledge data on the

TABLE 1 Ten most significant model parameters

Rank	Parameter	Meaning
1	$k_{f,5}$	Rate constant for the phosphorylation of active receptor.
2	L_s	Full-strength ligand concentration during stimulation.
3	$k_{f,4}$	Rate constant for the binding of ligand to precoupled receptor.
4	$k_{f,16}$	Rate constant for the degradation of IP3.
5	R_{pc}	Ratio of plasma membrane surface area to cytosolic volume.
6	G_d	Area density of free inactive G-protein.
7	$K_{d,2}$	Dissociation constant for the precoupling of receptor.
8	$k_{f,14}$	Rate constant for the nonstimulated IP3 production reaction.
9	$k_{f,8}$	Forward rate constant for the binding of calcium to PLC β .
10	$k_{r,8}$	Reverse rate constant for the binding of calcium to PLC β .

ET-1 stimulated responses of proteins upstream of IP3 do not currently exist. Model parameters were adjusted until the output from the model closely matched the experimental observations, to match the mouse atrial myocyte on stimulation by the specific extracellular ligand ET-1.

To achieve the fit, several parameters' values had to be changed from those derived from other sources. These changes are presented in Table 4.

A comparison of an IP3 transient from the model with experimentally determined IP3 time-course data from Jiang et al. on 100 μM of ET-1 stimulation is shown in Fig. 2. Simulation results were generated from the model defined in Table 3, with the parameters defined in Table 4, and $L_s = 0.100 \mu\text{M}$, $t_s = 30.0 \text{ s}$, to match the experimental protocol. The numerical solver used was an implicit Runge-Kutta method based on Radau quadrature, as described by Hairer and Wanner (41). Absolute and relative error tolerances were set at 10^{-9} . As can be seen, the model behavior closely matches experimental results.

A further comparison with IP3 transient data is shown in Fig. 3. Jiang et al. measured the IP3 concentration in cells 30 min after stimulation with various concentrations of ligand. To simulate this, the model's ligand stimulation strength (L_s) was varied at regular intervals from $1 \times 10^{-4} \mu\text{M}$ to $1.0 \mu\text{M}$, and the concentration of IP3 measured 1800 s (30 min) after ligand addition. Figs. 2 and 3 demonstrate that appropriate IP3 transient behavior is produced by the model.

Key drivers of the IP3 transient

The most significant parameters in terms of impact on the IP3 transient are listed in Table 1. Parameters were sorted by summing their proportional significance for each objective measure. A complete list of all model parameters and their

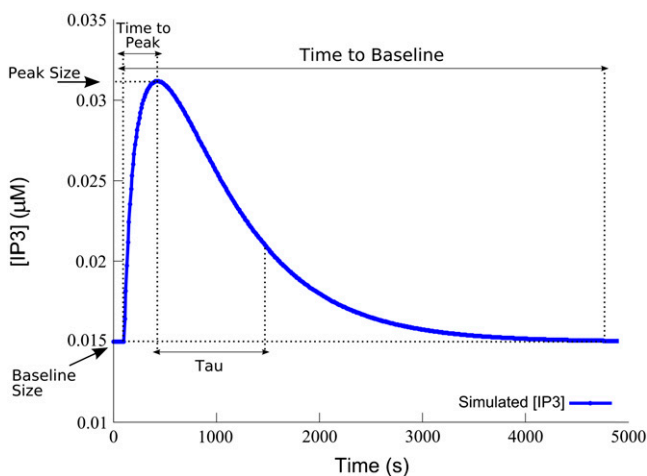


FIGURE 2 IP3 transient-based objective measures. Graphical depiction of the measures used to define the objective functions for the sensitivity analysis. Tau is the time point at which the transient dips beneath $1/e \times$ amplitude.

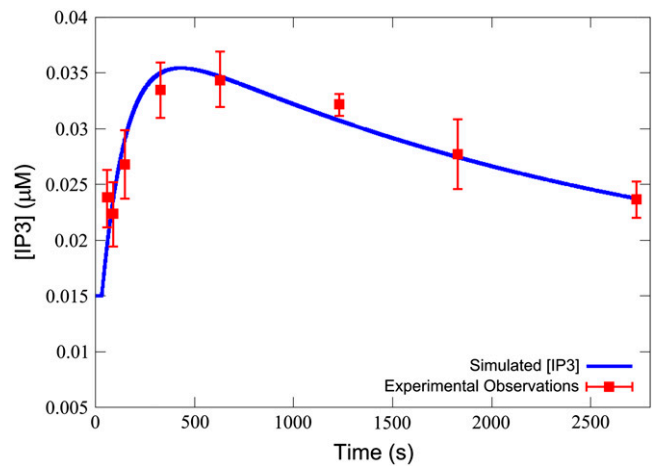


FIGURE 3 IP3 transient curve on ET-1 stimulation. The simulated IP3 transient closely matches experimental observations (40) on application of 100 nM ET-1. Simulations were performed with the equations as in Table 3 and the parameters and initial conditions as in Table 4. Additionally, $t_s = 30 \text{ s}$, and $L_s = 0.100 \mu\text{M}$.

significance scores can be found in Table S7 in the Supplementary Material.

The single most important parameter is the receptor phosphorylation rate constant ($k_{f,5}$). The quantity $k_{f,5}$ governs the reaction that terminates the signal by reducing the total available receptor density, and thus reducing the possibility of sarcolemmal signal transduction in response to extracellular hormonal stimulation. It is of critical importance for setting the Time-to-Baseline, as without a phosphorylation step the system would simply equilibrate based on the stimulation concentration of ligand and the transient would be constant.

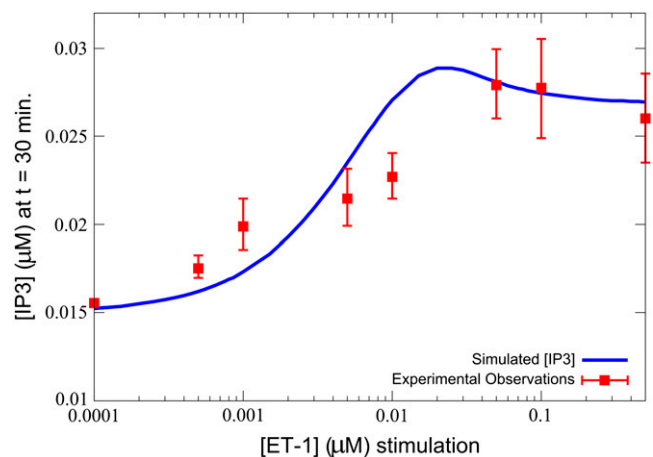


FIGURE 4 IP3 dose-response curve on ET-1 stimulation. The model also closely matches experimental observations (40) for the concentration of IP3, after 30 min, on stimulation by various concentrations of ET-1. Simulations were performed with the equations as in Table 3 and the parameters and initial conditions as in Table 4. Additionally, $t_s = 100 \text{ s}$, and the model was run until $(t - t_s) = 1800 \text{ s}$ (30 min of stimulation) for each of $L_s = 1 \times 10^{-4}$, 5×10^{-4} , 1×10^{-3} , 5×10^{-3} , 1×10^{-2} , 5×10^2 , 1×10^{-1} , and $5 \times 10^{-1} \mu\text{M}$.

Decreasing the phosphorylation rate via the $k_{f,5}$ parameter increases the tail as shown in Fig. 5. As can also be seen in that figure, a higher $k_{f,5}$ reduces the Time-to-Peak. While lowering $k_{f,5}$ increases the length of the transient's tail it also increases Tau. This is to be expected, however the increase in Tau is proportionally less than the increase in the tail length. Hence, over the range tested, the Tau-to-Tail Ratio reduces as $k_{f,5}$ increases. These three effects make the phosphorylation rate of the receptors crucial to determining the transient's behavior.

The following two parameters—the ligand strength (L_s) and the rate constant for the binding of ligand to precoupled receptor ($k_{f,4}$)—have virtually identical effects across all objective function measures (see Table S7 in the Supplementary Material for quantitative details). We consider each in turn.

It might be expected that the applied ligand concentration (L_s) is significant in determining the response. L_s is significant largely due to its effect on the Time-to-Peak, which is demonstrated in Fig. 6. For stimulation with lower ligand concentration, the transient flattens and takes longer to achieve its maximum. This is due to the effect that ligand concentration has on the phosphorylation of available receptor. With higher ligand concentration, more active receptor is immediately available for phosphorylation, which turns off the signal faster. For low ligand strength, less IP3 signal amplitude is achieved, but the receptor pool is not consumed as quickly. This can be seen from a plot of the percentage of phosphorylated receptor over time, as shown in Fig. 7 for the highest and lowest ligand strengths in Fig. 6.

The forward rate constant for the binding of ligand to precoupled receptor ($k_{f,4}$) also heavily influences the formation of activated receptors. This parameter has a large effect on

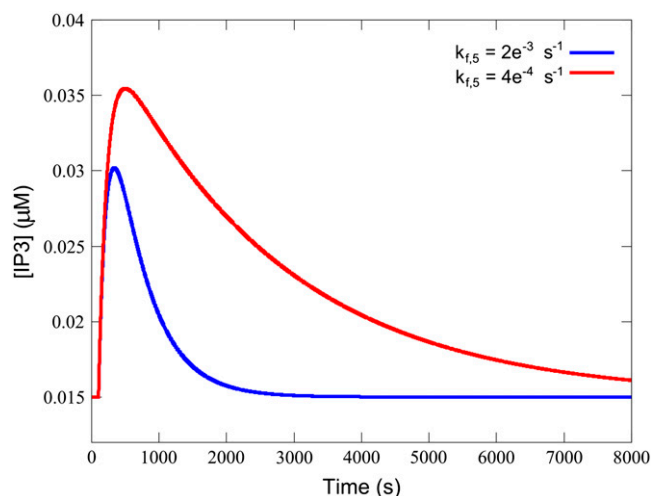


FIGURE 5 Decreased $k_{f,5}$ results in a higher peak and a longer time-to-baseline from peak. Simulations were performed with the equations as in Table 3 and the parameters and initial conditions as in Table 4. Additionally, $t_s = 100$ s, $L_s = 0.100$ μ M, and $k_{f,5}$ was varied as depicted in the legend.

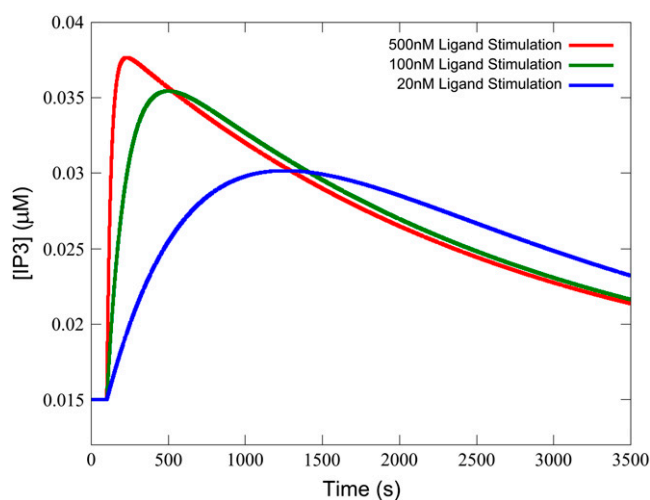


FIGURE 6 Decreasing ligand strength strongly effects Time-to-Peak. Lower ligand strength produces a slower rate of active receptor production, thus the transient takes more time to achieve its maximum. Simulations were performed with the equations as in Table 3 and the parameters and initial conditions as in Table 4. Additionally, $t_s = 100$ s and L_s was varied as depicted in the legend.

the Time-to-Peak. Examination of the changes in the membrane density of various species reveals that the IP3 transient closely follows the shape of the density curve on the active receptors (the product of reaction R4) (see Fig. 8). The parameter $k_{f,4}$'s effect on Time-to-Peak can thus be explained by its influence on the production of active receptor, which in turn leads to the peak for IP3.

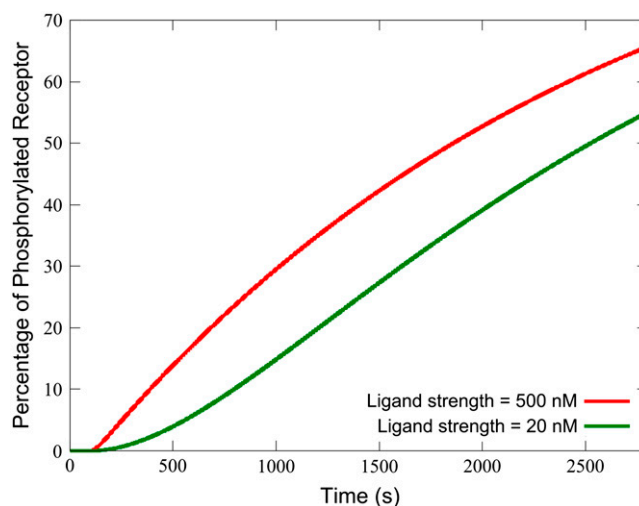


FIGURE 7 Higher ligand strength more readily increases phosphorylated receptor density. Although the long-term gradients for phosphorylated receptor density are similar for both high and low concentrations of ligand strength, a higher strength yields a much larger initial gain. Simulations were performed with the equations as in Table 3 and the parameters and initial conditions as in Table 4. Additionally, $t_s = 100$ s and L_s was varied as depicted in the legend.

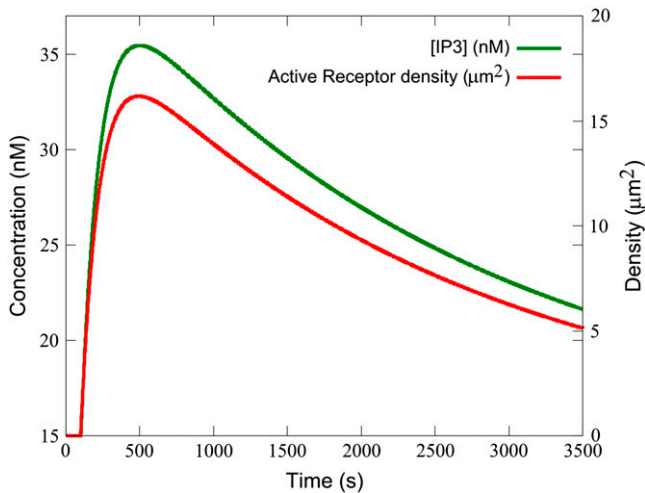


FIGURE 8 The IP3 transient follows the active receptor transient. Simulations were performed with the equations as in Table 3 and the parameters and initial conditions as in Table 4. Additionally, $t_s = 100$ s and $L_s = 0.100$ μM .

Both parameters also significantly influence the Time-to-Peak and the Tau-to-Tail Ratio. A higher peak due to high active receptor formulation (as increased by $k_{f,4}$, L_s and also the parameter G_d) leads sooner to a more rapidly decreasing transient, as receptors are more readily available to be phosphorylated faster. This gives a sharper peak earlier, with a longer post-peak tail and therefore a lower Tau-to-Tail Ratio, compared to a flatter transient with a longer time to peak, a shorter tail, and higher Tau-to-Tail Ratio when those parameters are lower. This is illustrated for $k_{f,4}$ specifically in Fig. 9. The same effect occurs when L_s or G_d are decreased (not shown).

The next most important parameter is the forward rate constant ($k_{f,16}$) for the degradation of IP3, which is the main consumer of IP3 in this system. The ratio of sarcolemmal surface area to cytosolic volume (R_{pc}) is also important as it determines the cytosolic flux in IP3 concentration resulting from a given surface area on the plasma membrane (a smaller cytosolic volume would yield a higher concentration change for the same IP3-producing sarcolemmal surface area). Hence this parameter has a direct effect on the concentration of IP3 produced for a given stimulus. Both these parameters mainly effect the IP3 Baseline Concentration and the Peak Concentration—one parameter affecting via IP3 degradation and the other affecting production, respectively.

The top five parameters together represent the most important determinants for each of the five objective functions— $k_{f,5}$ for Time-to-Baseline, L_s and $k_{f,4}$ both equally for each of Time-to-Peak and Tau-to-Tail Ratio, and both $k_{f,16}$ and R_{pc} for each of Baseline and Peak Concentration.

The value G_d represents the densities of a species required to form that mobile messenger—the amount of free $G_\alpha\text{GDP}$. G_d 's effects on Tau-to-Tail Ratio and Time-to-Peak is similar to the effect of $k_{f,4}$ or L_s , as has already been discussed, being

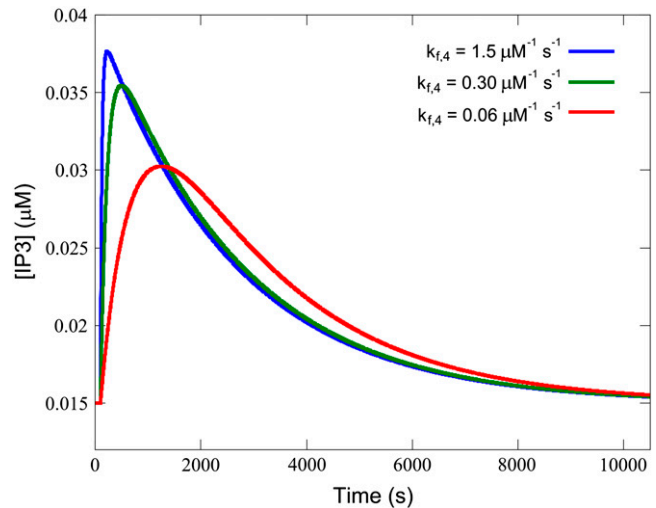


FIGURE 9 Higher $k_{f,4}$ reduces the Tau-to-Tail Ratio. Increased $k_{f,4}$ gives sharper peaks, but longer tails from the peak, and a lower Tau-to-Tail Ratio compared to flatter transients with a higher ratio when $k_{f,4}$ is decreased. Simulations were performed with the equations as in Table 3 and the parameters and initial conditions as in Table 4. Additionally, $t_s = 100$ s, $L_s = 0.100$ μM , and $k_{f,4}$ was varied as depicted in the legend.

a multiplicative factor in the forward rates of both reactions R2 and R3, which form active receptors.

$K_{d,2}$ has similar but less pronounced effects to G_d , which is due to it being a determinant of the rate of precoupled receptor formation, and therefore influences the rate of production of active receptors.

The basal IP3 production forward rate constant ($k_{f,14}$) is also important, largely for its effect on the Baseline Concentration. This is expected since the basal IP3 concentration is a balance of reaction R14 and the degradation rate as previously discussed.

The next two parameters of importance are the forward and reverse rate constants for the binding of calcium to PLC β . The PLC β -Ca²⁺ so produced is the only enzyme capable of producing IP3 in this system without ligand stimulation. Hence their effect on Baseline and Peak Concentrations, while less than that of other parameters such as $k_{f,16}$ and R_{pc} , is notable.

Together these are the most significant control parameters of the IP3 model. They are also, therefore, the key parameters to be determined experimentally for a species of interest, as they have the strongest effect on the time course of the IP3 transient after stimulation of the G_q protein-coupled receptors.

Angiotensin-II stimulation

The literature-derived and refinement-fitted parameter changes required to adjust the model (as discussed in Methods) for Ang-2 cell stimulation are shown in Table 2. A graph of the experimental observations together with the fitted IP3 transient is shown in Fig. 10.

TABLE 2 Parameters altered during refinement to angiotensin experimental data

Symbol	Meaning	ET-1 value	Ang-2 value	Source
$K_{d,1}$	Dissociation constant for the binding of ligand to the receptor with no attached G-protein.	$3.00 \times 10^{-5} \mu\text{M}$	$1.50 \times 10^{-3} \mu\text{M}^*$	Bers (28)
$K_{d,2}$	Dissociation constant for the binding of unbound receptor to G-protein.	$2.75 \times 10^4 \mu\text{m}^2$	$2.74 \times 10^4 \mu\text{m}^{2\dagger}$	
$K_{d,4}$	Dissociation constant for the binding of ligand to the receptor with attached G-protein.	$3.00 \times 10^{-5} \mu\text{M}$	$1.50 \times 10^{-3} \mu\text{M}^*$	Bers (28)
$k_{f,4}$	Forward rate for the binding of ligand to precoupled receptor.	$3.00 \times 10^{-1} \mu\text{M}^{-1} \text{s}^{-1}$	$6.02 \times 10^{-1} \mu\text{M}^{-1} \text{s}^{-1}$	(fitted value)
$k_{f,5}$	Receptor phosphorylation rate.	$4.00 \times 10^{-4} \text{s}^{-1}$	$6.22 \times 10^{-2} \text{s}^{-1}$	(fitted value)
$k_{f,6}$	G-protein dissociation rate from the activated receptor.	1s^{-1}	22.2s^{-1}	(fitted value)
R	Density of noncoupled receptors.	$13.9 \mu\text{m}^{-2}$	$2.93 \mu\text{m}^{-2}$	Bers (28)
R_g	Density of receptors coupled with G-proteins.	$5.06 \mu\text{m}^{-2}$	$1.07 \mu\text{m}^{-2}$	Bers (28)

*In keeping with the ET-1 model, $K_{d,1}$ and $K_{d,4}$ retain their equality to one another.

†Due to rounding for the values of R and R_g , the kinetic constant $K_{d,2}$ also had to be adjusted as the precise figure was closer to 27,400 than 27,500 μm^{-2} , to achieve the same steady-state levels of R and R_g .

Three parameters were adjusted during the refinement. An increase in $k_{f,5}$ is needed to reduce the length of the transient to the shorter Ang-2 response. A minor adjustment to $k_{f,4}$ (less than an order of magnitude) was also made. A third parameter was also modified—for forward rate constant for the dissociation of the messenger $G_\alpha\text{GTP}$ from active receptors ($k_{f,6}$). This modification was necessary due to the increased $k_{f,5}$, which results not only in a shorter tail, but a lower peak. By increasing $k_{f,6}$, more signal can be transferred to the PLC β module via the messenger $G_\alpha\text{GTP}$, raising the IP3 transient peak without greatly increasing the tail. This combination of parameter changes, in concert with those derived from the literature, was sufficient to explain the experimental data.

Thus, once we allow for different receptor densities and known kinetic differences, the difference between the ET-1- and Ang-2-induced IP3 transients can be explained solely in

terms of additional receptor kinetic changes in the phosphorylation rate (via rate constant $k_{f,5}$), the binding of extracellular ligand to the precoupled receptor ($k_{f,4}$) and the release of active G-protein ($k_{f,6}$).

DISCUSSION

We have presented the first model of the IP3 production system in the atrial cardiac myocyte. We used this model to 1), assess the key drivers of the IP3 transient system; and 2), hypothesize the kinetic mechanism that allows two different receptors to provoke different behaviors in the same downstream pathway.

The IP3 system

The sensitivity analysis showed that several parameters that we expected to be important were in fact significant, increasing our confidence in the model. It also rated some parameters unexpectedly high—indications which have led to further insights on the functioning of the IP3 production system.

That the phosphorylation rate of the receptor (via $k_{f,5}$) is of high importance is expected. There are two other switch-off points for the stimulated IP3 transient—the $G_\alpha\text{GTP}$ self-hydrolysis to $G_\alpha\text{GDP}$ when mobile (via $k_{f,7}$), or when bound to PLC β -Ca $^{2+}$ (via $k_{f,12}$ and $k_{f,13}$). The fact that the phosphorylation rate of the receptor is more important than these highlights the importance of the interface of the cell to the surroundings above the internal mechanisms, at least in this system.

It is also intuitive that the ligand strength (L_s) is important. What is perhaps less obvious but shown by the sensitivity analysis is that this effect seems to be due largely to the ligand's effect on precoupled receptor density as opposed to its effect on noncoupled receptor density. The impact of L_s is identical to that of the forward rate constant for the binding of that ligand to precoupled receptor. This is explainable by

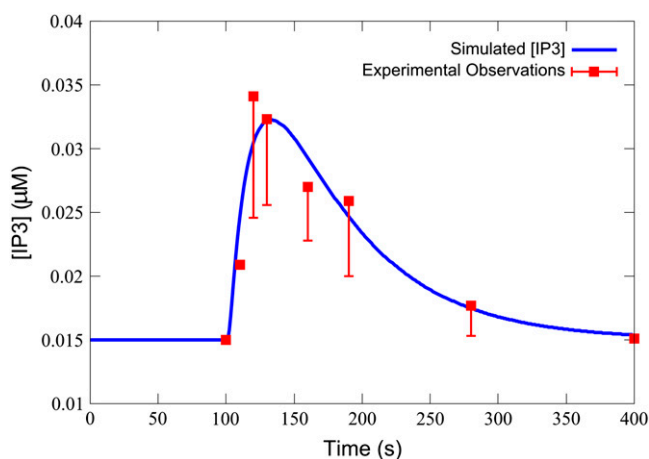


FIGURE 10 Simulated fit to the observations of Abdellatif et al. (39). The simulated transient matches the observations (39) for stimulation with 100 nM of Ang-2. Simulations were performed with the equations as in Table 3 and the parameters and initial conditions as in Table 4, and the Ang-2 values listed in Table 2. Additionally, $L_s = 100 \mu\text{M}$ and $t_s = 100 \text{s}$.

both being multiplicative factors in that reaction ($R4$). It is such reaction that is important for the formation of active receptors (R_{lg}) on stimulation by ligand. The noncoupled reaction ($R1$) is less important on the stimulation of ligand as a further reaction must then be carried out (reaction $R3$) for the G_α GDP to bind to the ligand-receptor complex before the receptor is active. In the precoupled state, the receptor becomes active much more readily and determines the responsiveness of the system far more significantly.

It seems likely that the effect on precoupled receptor density is also why the amount of G_α GDP and the dissociation constant for receptor precoupling ($K_{d,2}$) are significant at numbers six and seven in the top 10—which may have at first seemed puzzling. G_α GDP is a reactant for the formation of precoupled receptors (R_g), which in turn are reactants for that important reaction $R4$.

That the degradation rate of IP3 (via $k_{f,16}$) and geometric ratio of membrane area-to-cytosolic volume (R_{pc}) are important is also expected when their role in the degradation and production of IP3, respectively, is considered, as was noted above. That the parameters ($k_{f,8}$ and $k_{r,8}$) related to the formation of the basal PIP2-hydrolyser (P_c) and the subsequent hydrolysis reaction ($k_{f,14}$) are important is not surprising, given that the Baseline Concentration was one of the objective functions. The availability of P_c influences the resulting stimulated transient also, as mass of PLC β is conserved when forming the stimulated hydrolyser P_{cg} , and $k_{f,14}$ influences the difference between P_c activity and P_{cg} activity, having implications for the tail of the IP3 transient. Hence overall these are among the more significant parameters of the system.

Of the top seven parameters, five relate to the receptor kinetics. This highlights again the importance of the cell/environment interface in this system and indicates how a change in receptor density and kinetics from ET-1 to Ang-2 can alter the resulting IP3 transient to the extent observed experimentally.

Drivers of the angiotensin-II IP3 transient

Taken together, only parameters relating to the receptor kinetics and density have been altered to yield the fits to experimental data. Hence the model is consistent with the idea that a shorter IP3 transient from Ang-2 compared to ET-1 can be produced simply by a change in the type and number of receptors without the need for any other mechanisms.

The change in phosphorylation rate of active receptor (via constant $k_{f,5}$) is consistent with the observation that the receptor phosphorylation rates differ even between subtypes of the same receptor (42). As discussed above, this phosphorylation rate is the most important factor in determining the time for the transient to reach the baseline level again after stimulation. Therefore in determining the possible differences in receptor kinetics between ET-1 and Ang-2 binding receptors, an increase in the phosphorylation rate (to reduce the transient's time length) for Ang-2 receptors seems likely.

The increase required in the dissociation rate of active G-protein subunits from the receptor ($k_{f,6}$) suggests that, in cardiomyocytes, along with an increased phosphorylation rate (compared with endothelin receptors), the AT-1 receptor may also have an increased rate of G_α GTP dissociation from the activated receptor compared to that of the ET-1A receptor. This prediction, and the increase in the rate of binding of ligand to precoupled receptor ($k_{f,4}$), could be investigated experimentally.

We also refined the model to a second Ang-2 dataset from rat neonatal ventricular myocytes, that of Sadoshima and Izumo (43), which measured IP3 transients at two different concentrations of Ang-2. The experimental observations were too coarsely grained for our purposes to be confident about the

TABLE 3 IP3 model equations

$$\begin{aligned}
 C_c &= \frac{1}{V_c \times 6.022 \times 10^2} \\
 C_p &= \frac{1}{V_c \times R_{pc}} \\
 C_{pc} &= \frac{C_c}{C_p} \\
 L &= \frac{L_s}{(1.0 + e^{-80.0 \times ((t-t_s) - 0.05)})} \\
 &\quad \text{if } (t < (t_s + 0.15))(t \geq t_s), L_s; \text{ if } t \geq (t_s + 0.15), 0 \text{ otherwise.} \\
 k_{r,1} &= k_{f,1} \times K_{d,1} \\
 J_1 &= k_{f,1} \times R \times L - k_{r,1} \times R_l \\
 k_{r,2} &= k_{f,2} \times K_{d,2} \\
 J_2 &= (k_{f,2} \times R \times G_d - k_{r,2} \times R_g) \\
 \frac{dR}{dt} &= -(J_1 + J_2) \\
 J_3 &= k_{f,3} \times R_l \times G_d - k_{r,3} \times R_{lg} \\
 \frac{dR_l}{dt} &= J_1 - J_3 + J_6 \\
 k_{r,4} &= k_{f,4} \times K_{d,4} \\
 J_4 &= k_{f,4} \times L \times R_g - k_{r,4} \times R_{lg} \\
 \frac{dR_g}{dt} &= J_2 - J_4 \\
 \frac{dG_d}{dt} &= J_{12} + J_7 + J_{13} - (J_2 + J_3) \\
 J_5 &= k_{f,5} \times R_{lg} \\
 \frac{dR_{sp}}{dt} &= J_5 \\
 J_6 &= k_{f,6} \times R_{lg} \\
 \frac{dR_{lg}}{dt} &= J_3 + J_4 - (J_5 + J_6) \\
 J_7 &= k_{f,7} \times G_t \\
 \frac{dG_t}{dt} &= J_6 - J_7 - J_9 - J_{10} \\
 J_9 &= k_{f,9} \times P \times G_t - k_{r,9} \times P_g \\
 J_8 &= k_{f,8} \times P \times C_a - k_{r,8} \times P_c \\
 J_{10} &= k_{f,10} \times P_c \times G_t - k_{r,10} \times P_{cg} \\
 k_{r,11} &= k_{f,11} \times K_{d,11} \\
 J_{11} &= k_{f,11} \times P_g \times C_a - k_{r,11} \times P_{cg} \\
 J_{12} &= k_{f,12} \times P_{cg} \\
 J_{13} &= k_{f,13} \times P_g \\
 J_{14} &= \frac{k_{f,14} \times P_c \times PIP2}{\left(\frac{K_{m,14}}{C_{pc}} + PIP2\right)} \\
 J_{15} &= \frac{k_{f,15} \times P_{cg} \times PIP2}{\left(\frac{K_{m,15}}{C_{pc}} + PIP2\right)} \\
 \frac{dP}{dt} &= J_{13} - (J_9 + J_8) \\
 \frac{dP_g}{dt} &= J_9 - (J_{11} + J_{13}) \\
 \frac{dP_c}{dt} &= J_8 + J_{12} - J_{10} \\
 \frac{dP_{cg}}{dt} &= J_{10} + J_{11} - J_{12} \\
 J_{16} &= k_{f,16} \times IP3 \\
 \frac{dIP3}{dt} &= (J_{14} + J_{15}) \times C_{pc} - J_{16} \\
 \frac{dC_a}{dt} &= C_{pc} \times -1 \times (J_8 + J_{11})
 \end{aligned}$$

peak of the transient, but best fits were achieved with similar values for $k_{f,5}$ and $k_{f,6}$ (0.0421 s^{-1} compared with 0.0622 s^{-1} and 14.9 s^{-1} compared with 22.2 s^{-1} , respectively), increasing our confidence in the roles of the receptor phosphorylation and active G-protein dissociation rates.

The importance of the receptor phosphorylation rate, as evidenced both by the sensitivity analysis and its role in the fitting of the Ang-2 dataset, highlights the value of experimental measurement of this parameter for receptors of interest. Often experiments focus on determining the binding

TABLE 4 Model parameters and initial conditions

Symbol parameters	Description	Units	Value	Source
$k_{f,1}$	R1 forward rate constant	$\mu\text{M}^{-1} \text{ s}^{-1}$	3.00×10^{-4}	(fitted value)*
$K_{d,1}$	R1 dissociation constant	μM	3.00×10^{-5}	Bers (28)
$k_{f,2}$	R2 forward rate constant	$\mu\text{m}^2 \text{ s}^{-1}$	2.75×10^{-4}	Lukas (25)
$K_{d,2}$	R2 dissociation constant	μm^{-2}	27,500	Lukas (25)
$k_{f,3}$	R3 forward rate constant	$\mu\text{m}^2 \text{ s}^{-1}$	1.00	Lukas (25)
$k_{r,3}$	R3 reverse rate constant	s^{-1}	1.00×10^{-3}	Lukas (25)
$k_{f,4}$	R4 forward rate constant	$\mu\text{M}^{-1} \text{ s}^{-1}$	3.00×10^{-1}	(fitted value)†
$K_{d,4}$	R4 dissociation constant	μM	3.00×10^{-5}	Bers (28)
$k_{f,5}$	R5 forward rate constant	s^{-1}	4.00×10^{-4}	(fitted value)‡
$k_{f,6}$	R6 forward rate constant	s^{-1}	1.00	Lukas (25)
$k_{f,7}$	R7 forward rate constant	s^{-1}	1.50×10^{-1}	Lukas (25)
$k_{f,8}$	R8 forward rate constant	$\mu\text{M}^{-1} \text{ s}^{-1}$	1.67×10^{-2}	Lukas (25)
$k_{r,8}$	R8 reverse rate constant	s^{-1}	1.67×10^{-2}	Lukas (25)
$k_{f,9}$	R9 forward rate constant	$\mu\text{m}^2 \text{ s}^{-1}$	4.20×10^{-3}	Lukas (25)
$k_{r,9}$	R9 reverse rate constant	s^{-1}	1.00	Lukas (25)
$k_{f,10}$	R10 forward rate constant	$\mu\text{m}^2 \text{ s}^{-1}$	4.20×10^{-2}	Lukas (25)
$k_{r,10}$	R10 reverse rate constant	s^{-1}	1.00	Lukas (25)
$k_{f,11}$	R11 forward rate constant	$\mu\text{M}^{-1} \text{ s}^{-1}$	3.34×10^{-2}	See discussion under PLC β Cycling
$K_{d,11}$	R11 dissociation rate constant	μM	1.00×10^{-1}	Lukas (25)
$k_{f,12}$	R12 forward rate constant	s^{-1}	6.00	Lukas (25)
$k_{f,13}$	R13 forward rate constant	s^{-1}	6.00	See discussion under PLC β Cycling
$k_{f,14}$	R14 forward rate constant	s^{-1}	4.44×10^{-1}	See discussion under IP3 Production and Degradation
$K_{m,14}$	R14 K_m value	μM	19.8	Bhalla and Iyengar (49)
$k_{f,15}$	R15 forward rate constant	s^{-1}	3.80	(fitted value)§
$K_{m,15}$	R15 K_m value	μM	5.00	Bhalla and Iyengar (49)
$k_{f,16}$	R16 forward rate constant	s^{-1}	1.25	DOQCS ¹ database (50)
L_s	Ligand stimulation concentration	μM	varies	User-defined
$PIP2$	PIP2 density	μm^{-2}	4000	Xu et al. (51)
t_s	Time of stimulation	s	varies	User-defined
V_c	Cytosolic volume	μm^3	2549.3	Leri et al. (52), Bers (28)
Initial conditions				
Ca	Cytosolic Ca^{2+} concentration	μM	1.00×10^{-1}	Bers (28) (steady state)
G_d	G_α GDP density	μm^{-2}	10,000	Lukas (25) (steady state)
G_t	G_α GTP density	μm^{-2}	0.00	(unstimulated)
$IP3$	IP3 concentration	μM	0.015	See discussion under IP3 Production and Degradation
L	Ligand concentration (extracellular)	μM	0.00	(unstimulated)
P	PLC β density	μm^{-2}	90.9	Lukas (25) (steady state)
P_c	PLC β - Ca^{2+} density	μm^{-2}	9.09	Lukas (25) (steady state)
P_g	PLC β - G_α GTP density	μm^{-2}	0.00	(unstimulated)
P_{cg}	PLC β - Ca^{2+} - G_α GTP density	μm^{-2}	0.00	(unstimulated)
R	Noncoupled receptor density	μm^{-2}	13.9	Kobayashi (53) (steady state)
R_g	Precoupled receptor density	μm^{-2}	5.06	Kobayashi (53) (steady state)
R_l	Ligand-bound receptor density	μm^{-2}	0.00	(unstimulated)
R_{lg}	Active receptor density	μm^{-2}	0.00	(unstimulated)
R_{lep}	Phosphorylated receptor density	μm^{-2}	0.00	(unstimulated)
R_{pc}	Plasma membrane/cytosolic volume ratio	μm^{-1}	4.61	Bers (28)

All parameters are as at steady state. Fitted values are as a result of refinement to ET-1 data. See footnotes below.

*Altered from 1.68×10^{-2} (25).

†Altered from 16.8 (25).

‡Altered from 3.00×10^{-2} (25).

§Altered from 48.0 (49).

constants to certain ligands. As we have shown, for signal transduction the resulting intracellular signal is heavily influenced by the temporal dynamics of receptor activation, which is a balance between the binding of the ligand and the molecular events that switch-off active receptors. For the purposes of signal transduction, the determination of kinetic parameters pertaining to signal termination events may be even more important than the traditional focus on binding rates ($k_{f,5}$ was overall the most important parameter).

Future directions

We have concluded that the rate of receptor deactivation is crucial for determining the behavior of the stimulated transient. In vivo the signal is stopped by several receptor desensitization mechanisms, including phosphorylation, binding of an inhibitor protein to the receptor, and receptor internalization. The details of exactly which process leads to desensitization differ depending on cell and receptor type. For example, phosphorylation may not play a role in the internalization of β -2 adrenergic receptors, but may play a role in muscarinic acetylcholine receptors (44). Also, with respect to the path the receptor takes once internalized, even different isoforms of the same receptor can take different routes. For example, in Chinese hamster ovary cells, endothelin isoform A (ET-A) receptors were found to be routed to a recycling compartment while endothelin isoform B (ET-B) receptors appeared to be destroyed in internal lysosomes (45). It is also possible that recycling can occur via multiple pathways with different timescales, as it appears to do for the human V2 vasopressin receptor (46). The full desensitization-desensitization cycle of ET-A receptors in the cardiac myocyte is not completely understood. Therefore, in this work, receptor desensitization is modeled simply as a phosphorylation step. Experimentally, ET-A phosphorylation appears to be correlated with desensitization (27). There is, however, some evidence (42) that ET-A desensitization occurs via internalization rather than phosphorylation, hence what in the model is called phosphorylation may in reality be internalization.

While for the purposes of model functionality both abstractions are largely identical (being essentially a removal of receptors from availability), it may be useful to extend the model with details of this internalization and recycling, once known. This would allow the model to respond to multiple stimuli, as receptors could then get replenished post-phosphorylation. The question of how the longer timescale process of receptor recycling influences hypertrophic signaling could then also be explored.

This model assumes a resting level of calcium, similar to that employed in the experiments of Jiang et al. (40). In a beating heart, the calcium levels oscillate. From the sensitivity analysis the parameter Ca corresponding to cytosolic calcium concentration ranked 11th overall, due to its effects on Baseline and Peak Concentration of the IP3 transient, and

hence is likely to have a minor but measurable effect. It will therefore be interesting to explore the behavior of the model during a calcium oscillation and eventually couple to models of cell electrophysiology and excitation-contraction coupling (47,48). Comparing model results to experimental observations of IP3 transients in beating cells would extend our understanding of calcium handling in this system as it impacts on signal transduction.

The signal transduction pathway is complex and there are many kinetic parameters that could be measured. We present the top 10 parameters as those most likely to influence the IP3 transient formed in response to extracellular ligand. To confirm our understanding of this pathway in the cardiac myocyte it would be helpful to make experimental observations of these parameters and compare them to modeled values, thus refining the model as such data becomes available.

A further source of refinement would be transient data post ET-1 stimulation in the mouse atrial myocyte for proteins upstream of IP3; for example, free G_{α} GTP or calcium-bound PLC β . To our knowledge no such data exists, but such data could be used to constrain the model and refine its accuracy for behavior upstream of the IP3 transient.

The model predictions for the Ang-2 refinement are perhaps limited by the fact that we used data from rat ventricular myocyte, whereas the ET-1 stimulated model was developed in the mouse atrial myocyte. It is assumed that the Ang-2 induced IP3 transient would be sufficiently similar between the two cell types. To improve the validity of the refinement, it would be advantageous to conduct measurements of the Ang-2 induced IP3 transient in the mouse atrial myocyte and check that a similar refinement can be performed.

SUPPLEMENTARY MATERIAL

To view all of the supplemental files associated with this article, visit www.biophysj.org.

P.H. and E.J.C. thank the Maurice Wilkins Center for Molecular Biotechnology.

M.C. was supported by the Foundation for Research, Science and Technology of New Zealand through a Bright Futures Doctoral Scholarship.

REFERENCES

1. Heineke, J., and J. D. Molkentin. 2006. Regulation of cardiac hypertrophy by intracellular signaling pathways. *Nat. Rev. Mol. Cell Biol.* 7: 589–600.
2. Molkentin, J. D., J.-R. Lu, C. L. Antos, B. Markham, J. Richardson, J. Robbins, S. R. Grant, and E. N. Olson. 1998. A calcineurin-dependent transcriptional pathway for cardiac hypertrophy. *Cell.* 93:215–228.
3. Sugden, P. H. 1999. Signaling in myocardial hypertrophy: life after calcineurin? *Circ. Res.* 84:633–646.
4. Bare, D. J., C. S. Kettlun, M. Liang, D. M. Bers, and G. A. Mignery. 2005. Cardiac type 2 inositol 1,4,5-trisphosphate receptor: interaction and modulation by calcium/calmodulin-dependent protein kinase II. *J. Biol. Chem.* 280:15912–15920.
5. Hardt, S. E., and J. Sadoshima. 2002. Glycogen synthase kinase-3 β : a novel regulator of cardiac hypertrophy and development. *Circ. Res.* 90: 1055–1063.

6. Yamazaki, T., and Y. Yazaki. 2000. Molecular basis of cardiac hypertrophy. *Zeitschrift fr. Kardiologie*. 89:1–6.
7. Passier, R., H. Zeng, N. Frey, F. J. Naya, R. L. Nicol, T. A. McKinsey, P. Overbeek, J. A. Richardson, S. R. Grant, and E. N. Olson. 2000. CaM kinase signaling induces cardiac hypertrophy and activates the MEF2 transcription factor in vivo. *J. Clin. Invest.* 105:1395–1406.
8. Wilkins, B. J., and J. D. Molkentin. 2002. Calcineurin and cardiac hypertrophy: where have we been? Where are we going? *J. Physiol. (Lond.)*. 541:1–8.
9. Kohno, M., and J. Pouyssegur. 2003. Pharmacological inhibitors of the ERK signaling pathway: application as anticancer drugs. *Prog. Cell Cycle Res.* 5:219–224.
10. Crabtree, G. R. 1999. Generic signals and specific outcomes: signaling through Ca^{2+} , calcineurin, and NFAT. *Cell*. 96:611–614.
11. Ju, H., S. Zhao, P. S. Tappia, V. Panagia, and I. M. C. Dixon. 1998. Expression of Gq α and PLC- β in scar and border tissue in heart failure due to myocardial infarction. *Circulation*. 97:892–899.
12. Taylor, S. J., H. Z. Chae, S. G. Rhee, and J. H. Exton. 1991. Activation of the $\beta 1$ isozyme of phospholipase C by α subunits of the G $_q$ class of G-proteins. *Nature*. 350:516–518.
13. Wilkins, B. J., and J. D. Molkentin. 2004. Calcium-calcineurin signaling in the regulation of cardiac hypertrophy. *Biochem. Biophys. Res. Commun.* 322:1178–1191.
14. Crabtree, G. R., and E. N. Olson. 2002. NFAT signaling: choreographing the social lives of cells. *Cell*. 109:S67–S79.
15. Leinwand, L. A. 2001. Calcineurin inhibition and cardiac hypertrophy: a matter of balance. *Proc. Natl. Acad. Sci. USA*. 98:2947–2949.
16. Crampin, E. J., M. Halstead, P. Hunter, P. Nielsen, D. Noble, N. Smith, and M. Tawhai. 2004. Computational physiology and the physiome project. *Exp. Physiol.* 89:1–26.
17. Kakita, T., K. Hasegawa, E. Iwai-Kanai, S. Adachi, T. Morimoto, H. Wada, T. Kawamura, T. Yanazume, and S. Sasayama. 2001. Calcineurin pathway is required for Endothelin-1-mediated protection against oxidant stress-induced apoptosis in cardiac myocytes. *Circ. Res.* 88:1239–1246.
18. Sadoshima, J., Y. Xu, H. S. Stayter, and S. Izumo. 1993. Autocrine release of angiotensin II mediates stretch-induced hypertrophy of cardiac myocytes in vitro. *Cell*. 75:977–984.
19. Lijnen, P., and V. Petrov. 1999. Renin-angiotensin system, hypertrophy and gene expression in cardiac myocytes. *J. Mol. Cell. Cardiol.* 31:949–970.
20. Goutsouliak, V., and S. W. Rabkin. 1998. Comparison of angiotensin II type-1 and type-2 receptor antagonists on angiotensin II-induced IP3 generation in cardiomyocytes. *Gen. Pharmacol.* 30:367–372.
21. Touyz, R., and C. Berry. 2002. Recent advances in angiotensin II signaling. *Braz. J. Med. Biol. Res.* 35:1001–1015.
22. Hua, B., L.-L. Wu, D.-Q. Xing, J. Liu, and Y.-L. Zhao. 2004. Angiotensin II induced upregulation of G $_{\alpha q/11}$, phospholipase C $\beta 3$ and extracellular signal-regulated kinase 1/2 via angiotensin II type 1 receptor. *Chin. Med. J.* 117:88–93.
23. Mehta, P. K., and K. K. Griendling. 2007. Angiotensin II cell signaling: physiological and pathological effects in the cardiovascular system. *Am. J. Physiol. Cell Physiol.* 292:C82–C97.
24. Lloyd, C. M., M. D. B. Halstead, and P. F. Nielsen. 2004. CellML: its future, present and past. *Prog. Biophys. Mol. Biol.* 85:433–450.
25. Lukas, T. J. 2004. A signal transduction pathway model prototype I: from agonist to cellular endpoint. *Biophys. J.* 87:1406–1416.
26. Shea, L., and J. J. Linderman. 1997. Mechanistic model of G-protein signal transduction determinants of efficacy and effect of precoupled receptors. *Biochem. Pharmacol.* 53:519–530.
27. Freedman, N. J., A. S. Ament, M. Oppermann, R. H. Stoffel, S. T. Exum, and R. J. Lefkowitz. 1997. Phosphorylation and desensitization of human endothelin A and B receptors. Evidence for G-protein-coupled receptor kinase specificity. *J. Biol. Chem.* 272:17734–17743.
28. Bers, D. M. 2002. Excitation-Contraction Coupling and Cardiac Contractile Force, 2nd Ed. Kluwer Academic Publishers, New York.
29. Hunton, D. L., L.-Y. Zou, Y. Pang, and R. B. Marchase. 2004. Adult rat cardiomyocytes exhibit capacitative calcium entry. *Am. J. Physiol. Heart Circ. Physiol.* 286:H1124–H1132.
30. Haugh, J. M., A. Wells, and D. A. Lauffenburger. 2000. Mathematical modeling of epidermal growth factor receptor signaling through the phospholipase C pathway: mechanistic insights and predictions for molecular interventions. *Biotechnol. Bioeng.* 70:225–238.
31. Willars, G. B., S. R. Nahorski, and R. A. Challiss. 1998. Differential regulation of muscarinic acetylcholine receptor-sensitive polyphosphoinositide pools and consequences for signaling in human neuroblastoma cells. *J. Biol. Chem.* 273:5037–5046.
32. Remus, T. P., A. V. Zima, J. Bossuyt, D. J. Bare, J. L. Martin, L. A. Blatter, D. M. Bers, and G. A. Mignery. 2006. Biosensors to measure inositol 1,4,5-trisphosphate concentration in living cells with spatio-temporal resolution. *J. Biol. Chem.* 281:608–616.
33. Takanashi, M., and M. Endoh. 1992. Concentration- and time-dependence of phosphoinositide hydrolysis induced by endothelin-1 in relation to the positive inotropic effect in the rabbit ventricular myocardium. *J. Pharmacol. Exp. Ther.* 262:1189–1194.
34. Parkinson, P. A., H. Parfenova, and C. W. Leffler. 2000. Phospholipase C activation by prostacyclin receptor agonist in cerebral microvascular smooth muscle cells. *Proc. Soc. Exp. Biol. Med.* 223:53–58.
35. Morris, M. D. 1991. Factorial sampling plans for preliminary computational experiments. *Technometrics*. 33:161–174.
36. Campolongo, F., S. Tarantola, and A. Saltelli. 1999. Tackling quantitatively large dimensionality problems. *Comput. Phys. Commun.* 117:75–85.
37. Campolongo, F., J. Cariboni, A. Saltelli, and W. Schoutens. 2004. Enhancing the Morris Method. In *Sensitivity Analysis of Model Output*. K. M. Hanson, and F. M. Hemez, editors. SAMO 2004, Santa Fe, New Mexico.
38. Saltelli, A., S. Tarantola, F. Campolongo, and M. Ratto. 2004. *Sensitivity Analysis in Practice—A Guide to Assessing Scientific Models*. Wiley, New York.
39. Abdellatif, M. M., C. D. Neubauer, W. J. Lederer, and T. B. Rogers. 1991. Angiotensin-induced desensitization of the phosphoinositide pathway in cardiac cells occurs at the level of the receptor. *Circ. Res.* 69:800–809.
40. Jiang, T., E. Pak, H. Zhang, R. P. Kline, and S. F. Steinberg. 1996. Endothelin-dependent actions in cultured AT-1 cardiac myocytes: the role of the β isoform of protein kinase C. *Circ. Res.* 78:724–736.
41. Hairer, E., and G. Wanner. 1996. Solving ordinary differential equations. II. Stiff and differential-algebraic problems. In *Springer Series in Computational Mathematics*, Vol. 14, 2nd Ed. Springer, New York.
42. Cramer, H., W. Muller-Esterl, and C. Schroeder. 1997. Subtype-specific desensitization of human endothelin ETA and ETB receptors reflects differential receptor phosphorylation. *Biochemistry*. 36:13325–13332.
43. Sadoshima, J., and S. Izumo. 1993. Signal transduction pathways of angiotensin II-induced c-fos gene expression in cardiac myocytes in vitro. Roles of phospholipid-derived second messengers. *Circ. Res.* 73:424–438.
44. Ferguson, S. S. G., J. Zhang, L. S. Barak, and M. G. Caron. 1998. Molecular mechanisms of G-protein-coupled receptor desensitization and resensitization. *Life Sci.* 62:1561–1565.
45. Bremnes, T., J. D. Paasche, A. Mehlem, C. Sandberg, B. Bremnes, and H. Attramadal. 2000. Regulation and intracellular trafficking pathways of the endothelin receptors. *J. Biol. Chem.* 275:17596–17604.
46. Innamorati, G., C. Le Gouill, M. Balamotis, and M. Birnbaumer. 2001. The long and the short cycle. alternative intracellular routes for trafficking of G-protein-coupled receptors. *J. Biol. Chem.* 276:13096–13103.
47. Noble, D., and Y. Rudy. 2001. Models of cardiac ventricular action potentials: iterative interaction between experiment and simulation. *Philos. Trans. Roy. Soc. London A Math. Phys. Eng. Sci.* 359:1127–1142.
48. Crampin, E. J., and N. Smith. 2005. A dynamic model of excitation-contraction coupling during acidosis in cardiac ventricular myocytes. *Biophys. J.* 90:3074–3090.

49. Bhalla, U. S., and R. Iyengar. 1999. Emergent properties of networks of biological signaling pathways. *Science*. 283:381–387.
50. Sivakumaran, S., S. Hariharaputran, J. Mishra, and U. S. Bhalla. 2003. The database of quantitative cellular signaling: management and analysis of chemical kinetic models of signaling networks. *Bioinformatics*. 19:408–415.
51. Xu, C., J. Watras, and L. M. Loew. 2003. Kinetic analysis of receptor-activated phosphoinositide turnover. *J. Cell Biol.* 161:779–791.
52. Leri, A., S. Franco, A. Zacheo, L. Barlucchi, S. Chimenti, F. Limana, B. Nadal-Ginard, J. Kajstura, P. Anversa, and M. Blasco. 2003. Ablation of telomerase and telomere loss leads to cardiac dilatation and heart failure associated with p53 upregulation. *EMBO J.* 22:131–139.
53. Kobayashi, T., T. Miyauchi, S. Sakai, M. Kobayashi, I. Yamaguchi, K. Goto, and Y. Sugishita. 1999. Expression of endothelin-1, ETA and ETB receptors, and ECE and distribution of endothelin-1 in failing rat heart. *Am. J. Physiol. Heart Circ. Physiol.* 276:H1197–H1206.